PCCP

PAPER

View Article Online
View Journal | View Issue

Cite this: *Phys. Chem. Chem. Phys.*, 2016, **18**, 18342

Temperature-dependent dynamic correlations in suspensions of magnetic nanoparticles in a broad range of concentrations: a combined experimental and theoretical study

Alexey O. Ivanov,[a] Sofia S. Kantorovich,*[ab] Vladimir S. Zverev,[a] Ekaterina A. Elfimova,[a] Alexander V. Lebedev[c] and Alexander F. Pshenichnikov[c]

Received 26th April 2016,
Accepted 6th June 2016

DOI: 10.1039/c6cp02793h

www.rsc.org/pccp

The interweave of competing individual relaxations influenced by the presence of temperature and concentration dependent correlations is an intrinsic feature of superparamagnetic nanoparticle suspensions. This unique combination gives rise to multiple applications of such suspensions in medicine, nanotechnology and microfluidics. Here, using theory and experiment, we investigate dynamic magnetic susceptibility in a broad range of temperatures and frequencies. Our approach allows, for the first time to our knowledge, to separate clearly the effects of superparamagnetic particle polydispersity and interparticle magnetic interactions on the dynamic spectra of these systems. In this way, we not only provide a theoretical model that can predict well the dynamic response of magnetic nanoparticles systems, but also deepen the understanding of the dynamic nanoparticle self-assembly, opening new perspectives in tuning and controlling the magnetic behaviour of such systems in AC fields.

1 Introduction

In the last few decades, the amount of various technological and medical applications, relying on the dynamic response of magnetic nanoparticles, has steadily grown.[1–8] The complexity of the dynamic behaviour and the size of the particles, however, still pose a challenge for the development and bottom-up design of suitable smart magnetic soft nanomaterials. In molecular systems, AC susceptometry is a well-developed technique and is widely used to characterise the structure and the properties of polar liquids and electric dipolar soft matter.[9–14] In the case of magnetic relaxation in magnetic soft materials,[15–18] the response to an AC magnetic field strongly depends on the type of magnetic building blocks. Thus, for example, magnetic nanoparticles can be superparamagnetic or blocked.[19,20] In order to carefully control the properties of magnetic nanoparticles, various approaches have been recently proposed. Firstly, to change the shape of the particles, producing, for example, ellipsoids or rods,[21–29] or even more extravagant shapes such as cubes and stars.[30–33] Secondly, one can modify the internal structure of the particles by varying the chemical composition[34,35] or creating core–shell particles with various types of agglomerates serving as the core, thus providing particle internal anisotropy.[36–41] High demand for specific magnetic building blocks stems from the potential for diagnostics, therapy and *in vitro* analysis.[2,42–45] One of the examples, based on the dynamic magnetic relaxation of magnetic particles, is the so-called magnetic hyperthermia, usually applied alone or in combination with other treatments (phototermia or chemotherapy) to destroy cancer tumours.[46–51] In this method, it is absolutely essential to predict the frequencies and the characteristic relaxation scales of the systems depending on the particle anisotropy, granulometric composition and magnetic phase concentration.[52–54]

Traditional methods to do this are based on the Debye-like approach, in which magnetic nanoparticles are treated as an ideal superparamagnetic "gas".[53,55] Despite being very simple and clear, this method ignores the inherent and sometimes crucial interparticle correlations, providing as such the incorrect low-frequency behaviour. The latter is known to differ significantly from the so-called Langevin law, even for the systems where the dipolar interactions have the same order as thermal fluctuations.[56] Stronger interparticle or intermolecular interactions can lead to a broad range of structuring[57,58] and self-assembly[16,59,60] in soft matter, which cannot but affect the dynamics of these systems. Several attempts to incorporate the dipole–dipole interaction into the theoretical description of dynamic spectra are known.[61–64] The main conclusion of these

[a] *Ural Federal University, Lenin av. 51, 620000 Ekaterinburg, Russia*
[b] *University of Vienna, Sensengasse 8, 1090 Vienna, Austria. E-mail: sofia.kantorovich@univie.ac.at*
[c] *Institute of Continuous Media Mechanics, Ak. Koroleva str. 1, 614013 Perm, Russia*

works is that the dipolar correlations slow down the dynamics and result in larger relaxation time-scales.[61–63] The role of magnetic dipolar interactions in the specific absorption rate was actively studied both theoretically and experimentally.[65–68] In these studies, it was shown that the interparticle correlations might lead to the decrease, as well as to the increase, in the hypothermia efficiency depending on the magnetic particle size. This result together with the results of the study reported in ref. 69 underline the crucial part of polydispersity and interactions in the dynamic magnetic response and specific absorption rate. In general, it was shown both in simulations and experiments that complex nanoparticles with the ferromagnetic core and ferrimagnetic shell morphology can enhance the efficiency of hyperthermia.[70] Another combined theoretical and experimental investigation of hyperthermia was recently carried out at the level of mean-field for the model core–shell particle.[71] Unfortunately, these approaches cannot be directly applied to predict or analyse the dynamic spectra of magnetic dipolar nanoparticle systems, as they lack an intrinsic feature of the latter, namely, particle polydispersity. The numerical work on hyperthermia, in which polydispersity was addressed, showed that the dispersion of the local heating can change a lot with the particle average size.[72] To this extent, earlier this year, we put forward a new theoretical approach[73] based on the analytical solution of the Fokker–Plank equation with an additional term allowing for the interparticle interactions and system polydispersity. We tested our theory against Brownian dynamics computer simulations but only for the monodisperse case.[74]

In this manuscript we investigate, both theoretically and experimentally, how the solutions of polydisperse magnetic nanoparticles respond to a weak, linear polarised, harmonic, external field. Importantly, polydisperse magnetic nanoparticles suspended in a liquid carrier exhibit various magnetic relaxations depending on their size. It is also the particle size that, on the other hand, defines the strength of the magnetic dipole–dipole interaction. The latter, as already mentioned above, cannot but influence the dynamics of the system and may lead to a qualitative change in the response. Here, we accurately separate all these factors, obtaining seven samples with an identical particle size distribution different only in the nanoparticle volume fraction. Changing the frequency of the applied AC magnetic field from 10 to 10^5 Hz, we measure dynamic zero-field complex susceptibility at five different temperatures in the range of almost 100 K for all samples. We apply the previously developed theory to determine both its validity range and to explain the spectra observed in the experiment. Along with a very good agreement between our theoretical approach and the experimental data for dilute samples, we show that at high nanoparticle concentrations and low temperatures, the slow response seems to be caused by the presence of large particle structures in which magnetic moments are very strongly correlated and cannot react fast enough to the externally applied magnetic field.

The structure of the paper is as follows. First, we describe in detail our experimental approach. Next, we explain the basic idea of the theory. The main results of the paper are split into parts: we start with sample verification using static magnetic measurements, then we analyse the dynamic response of dilute systems and pinpoint the validity range of our theoretical model, and, finally, we analyse the magnetic dynamic susceptibilities of dense systems. The paper ends with a brief conclusion.

2 Experimental

For our experiments we chose to use a standard magnetite-in kerosene ferrofluid, with nanoparticles in it being stabilised by oleic acid. The average particle diameter is of the order of 10 nm. To get the basic samples we first use the known method of repeptisation or modification of magnetic fluid,[75,76] which involves the replacement of the carrier liquid. With this purpose, some amount of isopropyl alcohol in quantity enough for sedimentation of magnetite particles was added to the magnetite colloid, prepared using the chemical condensation technique. The sediment obtained was separated from the disperse media, washed several times with isopropyl alcohol (for the removal of free oleic acid), and, after drying, was again peptised in kerosene. Secondly, kerosene was added gradually under continuous mixing and careful control of nanoparticle peptisation. The sample, obtained in this way, is unavoidably polydisperse. Thus, the magnetic properties of the basic sample were carefully analysed to obtain the parameters for the nanoparticle size distribution. In order to follow the main idea of this study and to produce samples that differ only in the nanoparticle concentration, preserving the granulometric composition, we employed the dilution procedure[77] and verified it in the later work.[56] Monitoring of sedimentation stability was performed according to the equilibrium susceptibility by the method described earlier.[77] The dilution degree was selected in such a way that the initial static susceptibility of two subsequent samples differed by a factor of approximately 1.5 at room temperature. In order to check that the granulometric composition of all samples is preserved, we provide an additional analysis in Section 4.1. Static magnetisation was determined by the sweep method,[78] in which differential magnetic susceptibility $\chi_{\text{diff}}(H)$ of the fluid is directly measured and the magnetisation curve is obtained by numerical integration as follows:

$$M(H) = \int_0^H \mathrm{d}h\chi_{\text{diff}}(h), \tag{1}$$

where H is the magnetic field strength inside the fluid. The differential magnetic susceptibility was measured at a frequency of 0.5 Hz, *i.e.*, sufficiently low to ignore relaxation processes. The strength of the static component of the applied field, generated by a long liquid-cooled solenoid, did not exceed 300 kA m^{-1}. The strength of the probing AC field varied in the range from 300 to 3000 A m^{-1} depending on the permanent component. The measurement error of the magnetisation was not larger than 0.5%. The initial (zero-field) static susceptibility for the basic sample was 5.13 and the saturation magnetisation was 41.1 kA m^{-1}. The magnetisation curve can be found in Section 3.1. Dynamic susceptibility was measured using a thermostated

mutual induction bridge. The experimental set-up was tested extensively and ensures a high accuracy of the analysis of diluted solutions.[79] In addition, it allows us to measure at infra-low frequencies less than 10 Hz. The latter capability is especially important for the present study: it makes it possible to study the effects related to the slow magnetic relaxation and to elucidate the low-T behaviour of magnetic nanoparticles. Susceptibility measurements are based on the comparison between the output voltages of two mutual-induction coils, one of which contains the sample with a magnetic fluid. Depending on the frequency range two different analog-to-digital converters were used to measure the voltages. Due to the technical demand, the latter frequency ranges were 1–400 Hz and 100 Hz–100 kHz. In the experiment, the phase shift was measured. In this way, we reduced the error-bars for the real part of the dynamic spectrum up to 0.5% and for the imaginary part the measurement errors did not exceed 2%.

Dynamic susceptibility was measured at five different temperatures: T_1 = 232 K; T_2 = 252 K; T_3 = 273 K; T_4 = 300 K and T_5 = 337 K. According to the estimate, the temperature within the set-up in the experiment was defined with a precision of 0.2 K.

Finally, we created seven differently concentrated samples with an identical granulometric composition, for which we measured temperature-dependent series of both static and dynamic magnetic responses. The sketch, illustrating the experimental procedure, is shown in Fig. 1.

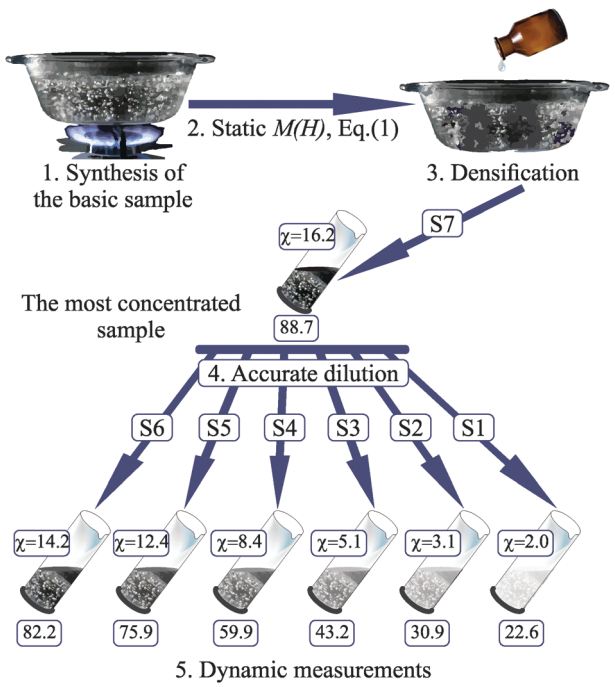

Fig. 1 The sketch of the experimental procedure. The seven samples are named S1–S7 starting from the most diluted to the most concentrated one. The corresponding values of the static initial susceptibility are provided for each sample, and the numbers below are the saturation magnetisations of the samples in kA m^{-1}; both susceptibility and magnetisation are measured at room temperature.

3 Theoretical approach

3.1 Static magnetic properties

The method to describe particle size polydispersity in magnetic fluids has been thoroughly studied by many authors (see ref. 75,76,80 and references therein). The common conclusion is that the nanoparticle size distribution is very close to the log-normal one. However, the latter was shown to have a clear disadvantage:[56] log-normal distribution has a slowly decaying long tail in the region of large particles, which leads to the overestimatoin of the mean dipole moment and as a result to the wrong prediction of the magnetic properties of the system. Hence, here we chose a more reliable gamma-distribution, for the first time applied to ferrofluids more than a decade ago:[77]

$$p(x) = \frac{1}{x_0}\left(\frac{x}{x_0}\right)^a \frac{\exp(-x/x_0)}{\Gamma(a+1)}. \quad (2)$$

Here and below, x denotes the diameter of the nanoparticle magnetic core, and x_0 and a are the distribution parameters characterising the maximum ax_0 and the width $(1 + a)^{-1/2}$, respectively.

If we assume that all nanoparticles do not interact with each other and independently react to an applied constant magnetic field H, then at a given temperature T, the magnetisation obeys the well-known Langevin law[81,82]

$$M_L(H) = n\int_0^\infty \left[\coth\frac{\mu_0\mu(x)H}{k_BT} - \frac{k_BT}{\mu_0\mu(x)H}\right]\mu(x)p(x)dx, \quad (3)$$

where k_BT is the thermal energy, μ_0 is the vacuum magnetic permeability, n stands for the number of particles per unit volume, and $\mu(x) = \pi M_0 x^3/6$ is the magnetic moment of a nanoparticle with magnetic core diameter x and saturation magnetisation of the bulk material M_0. Note that the latter changes with T. The Langevin zero-field (initial) susceptibility χ_L depends on the $p(x)$-weighted mean-squared magnetic moment $\langle\mu^2\rangle$ and has the form $\chi_L = n\mu_0\langle\mu^2\rangle/3k_BT$. This value determines the initial slope of the magnetisation curve (3). Linear n-dependence holds true for only the limit of infinite dilution. At finite concentrations the interparticle correlations cannot be neglected.[83–98] All of the aforementioned theories agree in the first-order correction to the Langevin law and provide the following expression for the static initial susceptibility of the samples:

$$\chi_1(0) = \chi_L(1 + \chi_L/3), \quad (4)$$

where zero specifies the zero frequency of the AC probing field. This expression can be accurately derived in the framework of the modified mean-field approach of the first order (MMF1).[99] This first-order expansion was shown to adequately describe the magnetic response of the low-concentrated ferrofluids at room temperature, but to be insufficient while dealing with low T and higher n, as those introduced in the previous section. For this reason, to describe accurately the static magnetic properties of our samples, we use the extension of MMF1, whose applicability is well extended to the range of parameters of interest. The second order correction to the Langevin law, similar to the first order one, is based on the assumption that

the particles in the system react not only to the applied magnetic field, but are also subjected to the effective field, generated by all other dipoles in the system. In the MMF2 (modified mean-field of the second order) approach, the total field acting on a random particle contains more terms that its MMF1 analog and can be written as[92,99]

$$H_e(H) = H + \frac{1}{3}M_L(H)\left[1 + \frac{1}{48}\frac{dM_L(H)}{dH}\right]. \quad (5)$$

As a result, the magnetisation $M(H)$ and the initial susceptibility are

$$M(H) = M_L(H_e(H)), \quad \chi_2(0) = \chi_L\left[1 + \frac{\chi_L}{3} + \frac{{\chi_L}^2}{144}\right]. \quad (6)$$

Earlier we used MMF2 approach (5), (6) to extract $p(x)$ from magnetic measurements.[56] This technique is called magneto-granulometric analysis. Its main idea is based on finding x_0 and a from the measured initial susceptibility and saturation magnetisation solving the system of algebraic equations. The obtained distribution is later verified by plugging it into eqn (6) and comparing with the whole measured magnetisation curve. In our case, when six different samples were obtained *via* dilution of the most concentrated one, the additional check of the granulometric composition preservation was performed through comparing theoretically predicted and measured initial static susceptibilities for all samples in a broad range of temperatures $[T_1–T_5]$. For such a strong temperature variation, one needs to take into account the change in the number concentration n due to the carrier liquid thermal expansion and the T-dependence of the nanoparticle core magnetisation M_0:[34,100,101]

$$n(T) = n(T_*)[1 - \beta_1(1 - \varphi)(T - T_*)], \quad (7)$$

$$M_0(T) = M_0(T_*)(1 - \beta_2 T^2)/(1 - \beta_2 T_*^2),$$

where T_* stands for a reference temperature, $\beta_1 \approx 0.97 \times 10^{-3}$ 1/K is the coefficient of thermal expansion of the carrier liquid (kerosene), and $\beta_2 \approx 8 \times 10^{-7}$ 1/K^2 is the temperature correction coefficient for M_0 (magnetite). In these expressions, the magnetic nanoparticles are considered as thermally incompressible (as compared to the carrier liquid), and φ stands for the volume fraction of metallic nanoparticles. For magnetite nanoparticles we use below the value $M_0(T_* = 293) = 480$ kA m^{-1} at room temperature.

3.2 Weak field dynamic magnetic response

One of the unique features of the magnetic nanoparticle suspensions is a coexistence of two different magnetic relaxation mechanisms: Brown and Neél.[102,103] The first one involves the mechanical rotation of a nanoparticle as a rigid body to reorient the magnetic moment frozen within the crystallographic axes. Brownian rotation has a characteristic time $\tau_B = 3\eta v_h/k_BT$, which is determined by the particle hydrodynamic volume $v_h = \pi {x_h}^3/6$ (x_h being a hydrodynamic particle diameter), and the carrier viscosity η. This mechanism is realised by mainly large particles, whose magnetic anisotropy energy is high enough to suppress thermal fluctuations of the nanoparticle magnetic moment, *i.e.* to avoid superparamagnetic behaviour. The probability for a nanoparticle to be superparamagnetic is defined by the ratio $\sigma = Kv/k_BT$, where $v = \pi x^3/6$ in the magnetic core volume and K denotes the internal anisotropy constant. The magnetic moment in this case relaxes *via* the Neél mechanism, which does not involve the rotation of the particle as a whole and has a characteristic time[53,104]

$$\tau_N = \tau_0\frac{\exp(\sigma) - 1}{2\sigma}\left[\frac{\sigma + 1}{\sigma}\sqrt{\frac{\sigma}{\pi}} + 2^{-\sigma-1}\right]^{-1} \quad (8)$$

that depends on the particle characteristic relaxation time scale $\tau_0 \sim 10^{-9}$ s. Note that η, τ_0 and K change with temperature. In this study, we used experimental values for the dynamic effective viscosity; for τ_0 we used the $1/T$ dependence.[105] For the anisotropy constant K several approximations are known. One of those is the power-law relation with the bulk magnetisation[106] $K(T) \sim [M_0(T)]^\kappa$, where for a simple uniaxial crystal $\kappa = 3$. Another, more accurate one, predicts a non-monotonic dependence instead.[107] Both of them, however, state the growth of K on cooling in the studied temperature range.

For each magnetic nanoparticle in the system, its most probable relaxation is the shortest of τ_N and τ_B, which is why it is common to use the following expression for the relaxation time as a function of the particle size:

$$\tau(x) = \tau_N\tau_B/(\tau_N + \tau_B). \quad (9)$$

In the traditional Langevin-like assumption of non-interacting magnetic nanoparticles, one can write the dynamic zero-field susceptibility in a classical Debye[108] form, where the relaxation times enter as simple statistical weights:

$$\chi_D(\omega) = \chi_D'(\omega) - i\chi_D''(\omega),$$

$$\chi_D'(\omega) = \frac{\mu_0 n}{3k_BT}\int_0^\infty \frac{\mu^2(x)}{1 + \omega^2\tau^2(x)}p(x)dx,$$
$$\chi_D''(\omega) = \frac{\mu_0 n}{3k_BT}\int_0^\infty \frac{\mu^2(x)\omega\tau(x)}{1 + \omega^2\tau^2(x)}p(x)dx. \quad (10)$$

Even though the usage of the expressions (10) seems to be overwhelming, there are at least two main problems to be considered. Firstly, the static limit of the Debye susceptibility is nothing but χ_L, which can only describe the initial susceptibility of an ideal superparamagnetic gas. Secondly, for a given $p(x)$, the position of the $\chi_D''(\omega)$ maximum does not change with nanoparticle concentration, which contradicts the experimental results (known[16] and presented below).

Recently, we extended the MMF1 approach (4) to the case of the weak AC magnetic field.[73] This work resulted in the expressions for the dynamic magnetic response as an expansion in Debye susceptibilities:

$$\chi'(\omega) = \chi_D'(\omega) + \frac{1}{3}\left[{\chi_D'}^2(\omega) - {\chi_D''}^2(\omega)\right], \quad (11)$$

$$\chi''(\omega) = \chi_D''(\omega)\left[1 + \frac{2}{3}\chi_D'(\omega)\right].$$

Importantly, these expressions are the exact results of the first-order perturbation theory and have the quadratic precision in n. Besides, in the zero-frequency limit, the real part $\chi'(\omega \to 0) = \chi_1(0)$ (see eqn (4)). Unlike earlier attempts to allow for interparticle interactions,[61–64] this approach does not contain any Weiss-type singularities and properly allows for nanoparticle polydispersity. The latter is of crucial importance for describing real experimental systems. At the same time, these expressions could not be applied to concentrated systems, since the region of validity of the MMF1 model is limited by the value of the Langevin susceptibility $\chi_L < 10$ (compare eqn (4) and (6)).

4 Results and discussions

4.1 Verifying the granulometric composition upon dilution: static case

The measured static magnetisation curve of the basic sample is shown in Fig. 2. The magnetogranulometric analysis used allows for the following parameters of the basic sample to be found: nanoparticle concentration $n = 12.6 \times 10^{23}$ m^{-3}, gamma-distribution parameters $x_0 = 0.83$ nm and $a = 11.15$. The distribution maximum is 9.3 nm and the mean diameter of the nanoparticle magnetic core is 10.1 nm, so the majority of particles are very small. The distribution width is approximately 0.28, meaning that the distribution is rather narrow (Fig. 2, inset), and the large particle fraction $\sim$20 nm does not exceed 1%. Using the parameters obtained in MMF2 magnetisation (5), (6) we obtain a very accurate description of the experimental magnetisation curve in Fig. 2 in the whole range of magnetic field strengths. It should be noted that the Langevin magnetisation underestimates the experimental data significantly.

To verify the obtained nanoparticle granulometric composition, we calculated the temperature dependence of the static initial magnetic susceptibility for all samples S1–S7 on the basis of MMF2 theory (6) under the conditions when the temperature corrections (7) are taken into account. The comparison is shown in Fig. 3 for the whole experimental temperature range T_1–T_5. The close agreement between experimental data and theoretical predictions substantiates our assumption about preserving the nanoparticle polydispersity in the samples under study. In addition, it is worth mentioning that the static magnetic properties of our samples are quite far from the ideal paramagnetic behaviour as seen from the inset of Fig. 3, where the measured susceptibility (triangles) increases with concentration much faster than the linear Langevin dependence (crosses).

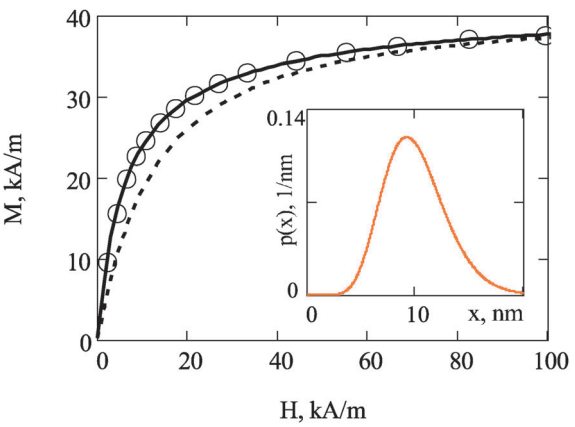

Fig. 2 Static magnetisation curve for the basic sample (T = 285 K). The symbols show the experimental data; the solid line is the MMF2 theoretical prediction (6); the dashed line describes $M_L(H)$ (3) for the same $p(x)$. Inset: Magnetic core size distribution $p(x)$ with parameters determined from the magnetogranulometric analysis (x_0 = 0.83 nm, a = 11.15).

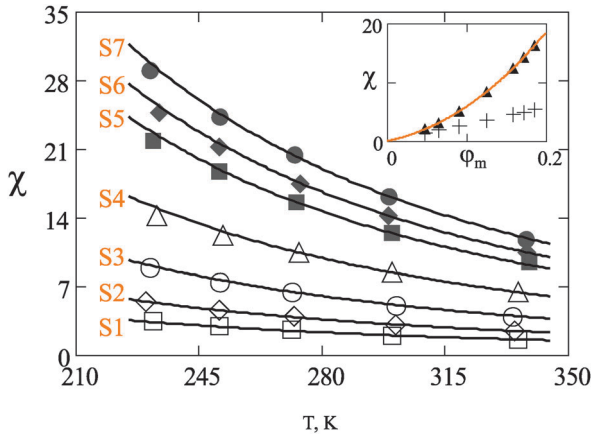

Fig. 3 Temperature dependence of the static initial magnetic susceptibility for samples S1–S7. Experimental data are shown by different symbols; solid lines represent the results of eqn (6) for the corresponding sample parameters with an identical $p(x)$. Inset: Static initial magnetic susceptibility *versus* magnetic phase concentration φ_m at 300 K; experimental data are given by triangles; the curve represents the MMF2 prediction (6); the crosses show the corresponding values of the Langevin susceptibility, calculated for samples S1–S7 with known $p(x)$.

4.2 Dynamic spectra analysis

4.2.1 Experimental curves. We start describing the dynamic magnetic properties with the most concentrated samples S4–S7 (Fig. 4). Even though, if comparing plots for S4–S7, the low-frequency limit of the susceptibility increases basically by a factor of 2, and the particle concentration differs by more than 50%, the qualitative behaviour at each given T is the same for all samples. At the lowest temperature 232 K (crosses) the real part χ' of the initial susceptibility decreases logarithmically with the probing field frequency f starting from approximately 100 Hz. The corresponding experimental values for these samples are situated on some straight lines (note that a logarithmic scale is used for the frequency axis). In the range of 10 Hz the trend to the low-f limit is rather weakly pronounced. At the same time, for the lowest temperature, the imaginary part χ'' of the susceptibility exhibits a small maximum for frequencies of the order of 1 kHz. In the frequency range studied, the decrease of χ' becomes smoother on heating. For the highest temperature 337 K (orange circles) the real part remains basically constant for each sample. Simultaneously, the imaginary part decreases with T, so that no actual energy absorption by these magnetic fluids can be observed in the frequency range below 100 kHz. The dynamic susceptibility of

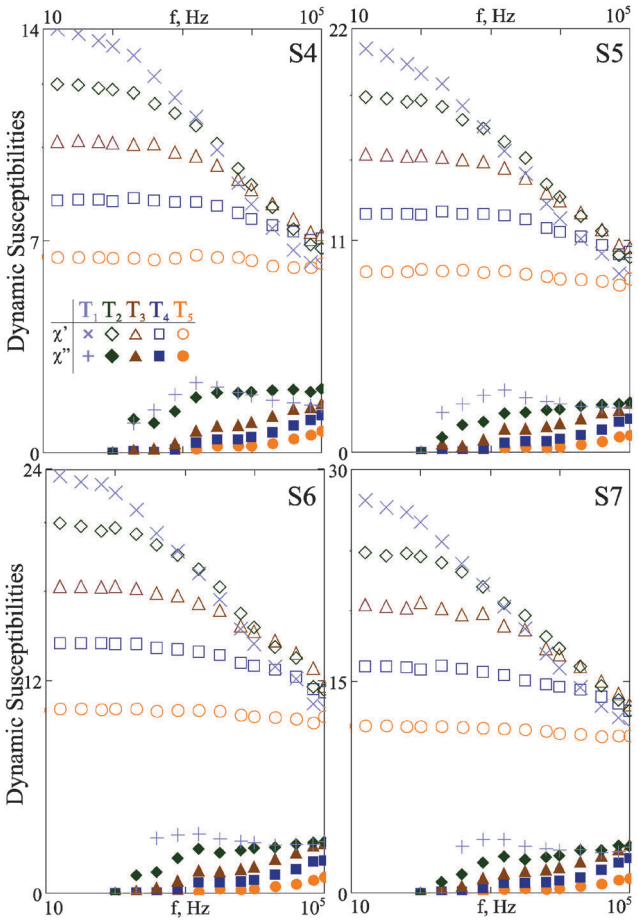

Fig. 4 Dynamic spectra of samples S4–S7. Both real χ' and imaginary χ'' parts of the zero-field dynamic susceptibility are presented at different temperatures T_1–T_5 as indicated in the legend. Experimental data are shown by symbols.

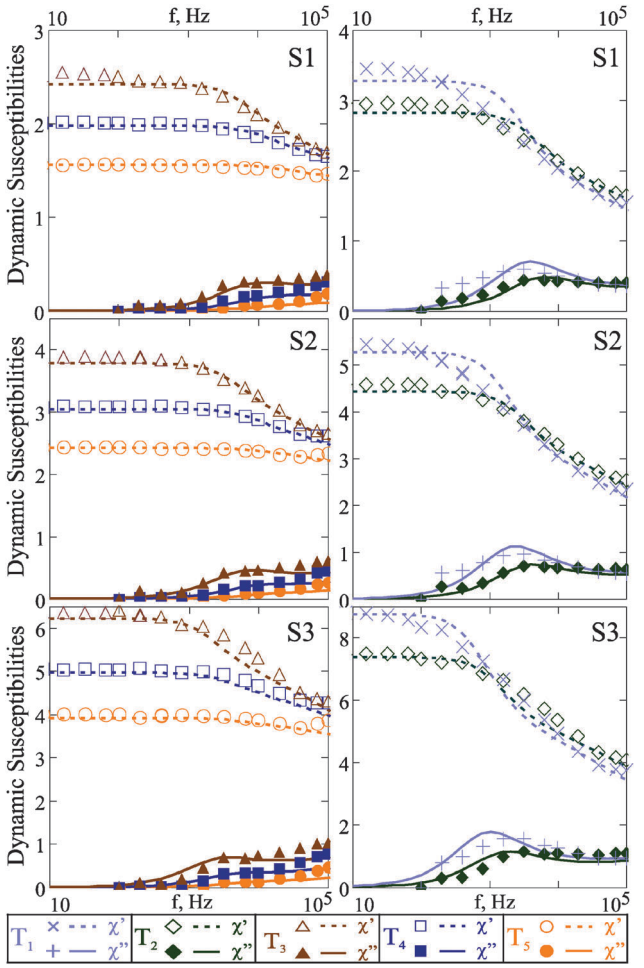

Fig. 5 Dynamic spectra of samples S1– S3. Both real χ' and imaginary χ'' parts of the zero-field dynamic susceptibility are presented at different temperatures T_1–T_5 as indicated in the legend. The symbols show the measured data, the results of approach (11) are plotted with lines.

samples S1–S3 with lower nanoparticle concentrations exhibits a similar behaviour, as seen from Fig. 5. The difference is that the real parts of these samples saturate at frequencies higher than that of concentrated samples. The region of saturation starts in this case around 1 kHz.

Analysing the discovered tendency, we must conclude that at higher temperature the magnetic moments of all nanoparticles are rotating at a time scale smaller than 10^{-5} s, and so even for the frequency 100 kHz the magnetic response of all samples is close to the static one. However, hundred degrees temperature decrease drastically changes the situation for concentrated samples. At the lowest temperature magnetic fluids S1–S7 seem to contain some structural units, whose magnetic relaxation is very slow, up to 10^{-1} s. On the one hand, these units are most probably temperature reversible: we see no signature of slow magnetic relaxations at $T > T_2$. On the other hand, the impact, if any, of these units on the static magnetic susceptibility turns out to be too small to be measured. One of the possible explanations for the arising low-frequency response can be related to the fact that magnetic moments are forming a certain arrangement with strong internal correlations and low overall intrinsic magnetisation. Topologically similar structures were recently observed in Monte Carlo simulations,[109–111] where dipolar hard spheres at low temperatures form percolating networks, in which the building blocks possess a vanishing magnetic moment. The existence of "magnetically slow" units will be assessed in more detail in the following sections.

4.2.2 In the mean-field range. As mentioned above, MMF1 is only valid for the samples with $\chi_L \ll 10$. This allows us to apply the dynamic MMF1 model from eqn (11) to at most first three samples (S1–S3). For this purpose, we use the obtained distribution $p(x)$ and known experimental values for the effective viscosity (see Table 1), assuming the existence of the non-magnetic layer on the nanoparticle surfaces of width 3 nm (2.2 nm of the oleic acid shell attached to the surface of the

Table 1 Sample parameters: effective viscosity and anisotropy constant

		T_1	T_2	T_3	T_4	T_5
η, mPa s	S1	6.1	4.0	2.7	1.7	1.1
	S2	9.3	5.7	3.7	2.3	1.4
	S3	21.1	12.6	8.0	4.7	2.9
K, kJ m^{-3}		19	17	15	13	11

nanoparticle and the disordered surface of the magnetic core, whose thickness can be estimated to be of the order of the lattice constant, *i.e.* ~0.8 nm for magnetite[75,76,80]). The value of anisotropy constant K was chosen as the fitting parameter in the range of 10–30 kJ m^{-3}.[15] Theoretical curves are plotted in Fig. 5, and the fitted K for each temperature are given in Table 1.

The agreement between the dynamic MMF1 model and the experimental data for S1 is quite accurate, both for the real part and for the imaginary part for temperatures T_2–T_5. Some minor disagreement occurs for the real part spectrum at the lowest temperature T_1.

Based on this success, we applied the dynamic MMF1 model with the same found $K(T)$ values (Table 1) to describe the dynamic spectra of samples S2 and S3. In general, we should conclude that for also these samples, at high temperatures T_3–T_5, our theory describes the experimental results very nicely. An expected tendency is observed: the higher the nanoparticle concentration, the larger the deviations of the experimental data from the theoretical predictions. It is obviously caused by the violation of the validity limits of the MMF1 approach.

To clarify the physical reasons for the spectral changes with temperature we calculated the size dependence of both relaxation times τ_N and τ_B, plotted in Fig. 6a, as well as the effective relaxation time $\tau(x)$ from (9). One can see that, at the lowest temperature, for sample S1, the transition between two mechanisms occurs for the particles with magnetic core diameter $16 < x < 18$ nm. With increase in temperature this crossover shifts towards larger particles. At T_5, one can barely see magnetic nanoparticles with Brownian relaxation smaller than 24 nm. It is worth mentioning here that, looking at the magnetic core size distribution presented in the inset of Fig. 2, it is clear that the portion of particles with $x > 24$ nm is simply negligible in the systems under study. This explains why the imaginary part of the susceptibility at T_5 exhibits no maximum in the range of frequencies plotted in Fig. 4 and 5 and the real part for all samples at T_5 stays practically constant. In other words, the energy absorption at high temperatures occurs only at frequencies of the order of 100 kHz, and there are no signs of clustering, induced by increasing nanoparticle concentration, in this T-regime. Once the temperature starts decreasing, the interparticle correlations come into play: the dynamic spectra stop being directly related to the individual nanoparticle relaxation times. However, in the intermediate temperature regime, there is still no reason to talk about any type of self-assembly in the nanoparticle suspension, otherwise the mean-field approach would have failed to describe the dynamic response. Indeed, we observe that the mean-field approach of (11) starts deviating from the experimental data at the lowest T_1 even for the most dilute sample S1. This limitation not only sets the range of our theoretical approach validity, but also indicates the range of nanoparticle concentrations and temperatures at which the intensity of the interparticle correlations, both short- and long-range ones, becomes high enough to basically suppress the individual relaxations replacing them by very complex collective dynamics.

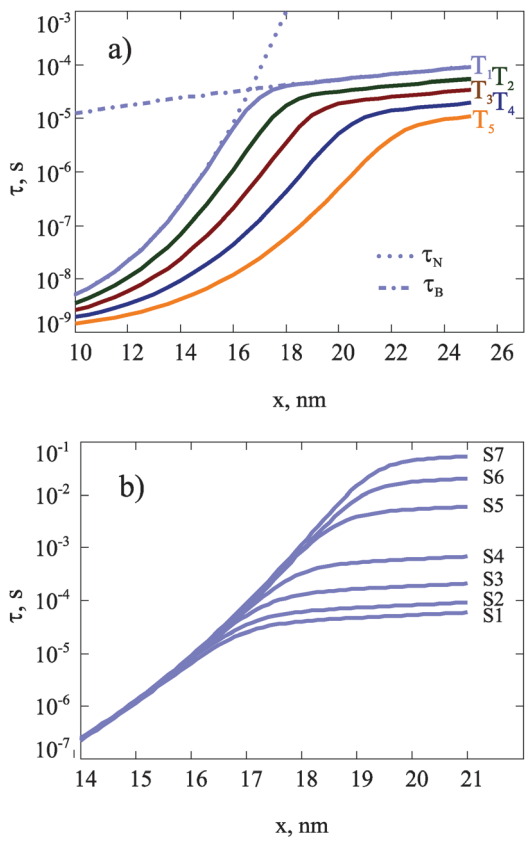

Fig. 6 Relaxation time of a nanoparticle *versus* its magnetic core diameter x. (a) Sample S1, temperatures are indicated in the plot. The solid lines are $\tau(x)$ from (9) for the corresponding temperatures; τ_N is plotted with the dotted line for T_1; τ_B is presented with the dashed-dotted line for T_1. (b) Samples S1–S7, as indicated in the plot, $T = T_1$.

4.2.3 Beyond mean field. In the static case, at high and moderate values of T, it is known that on increasing the nanoparticle concentration, the MMF1 model described by eqn (4) underestimates static magnetic susceptibility as it neglects multi-particle correlations. These correlations can be taken into account analytically only partially, and the MMF2 (6) model proves to be a reasonable extension, for example. Unfortunately, at the moment, there is no clarity of how to apply this type of expansion to the case of the applied AC magnetic field. One can, though, speculate here, looking at T_4–T_5 curves in Fig. 4, that this kind of approach can still work. As for lower temperatures, a detailed comparison of Fig. 4, 6b and 7 and the inset of Fig. 2 reveals a different tendency. In concentrated samples S4–S7, the low-T low-f relaxation becomes more pronounced with increasing n (see crosses in Fig. 4). At the same time, the relaxation times in this temperature regime, as shown in Fig. 6b, also increase drastically with nanoparticle concentration and even go above 10^{-2} s. At this frequency one can see a clear decay of χ' in Fig. 4. However, one cannot attribute this decay exclusively to the particles with slow magnetic relaxation: looking at χ'' for T_1, shown in Fig. 7, one sees that the maximum is at a frequency of $\sim 10^3$ Hz, but this maximum is highly pronounced and shifts to higher frequencies upon dilution. The latter, besides demonstrating the necessity to include dipolar correlations while describing the dynamic response (in contrast to the Debye approach), evidences the

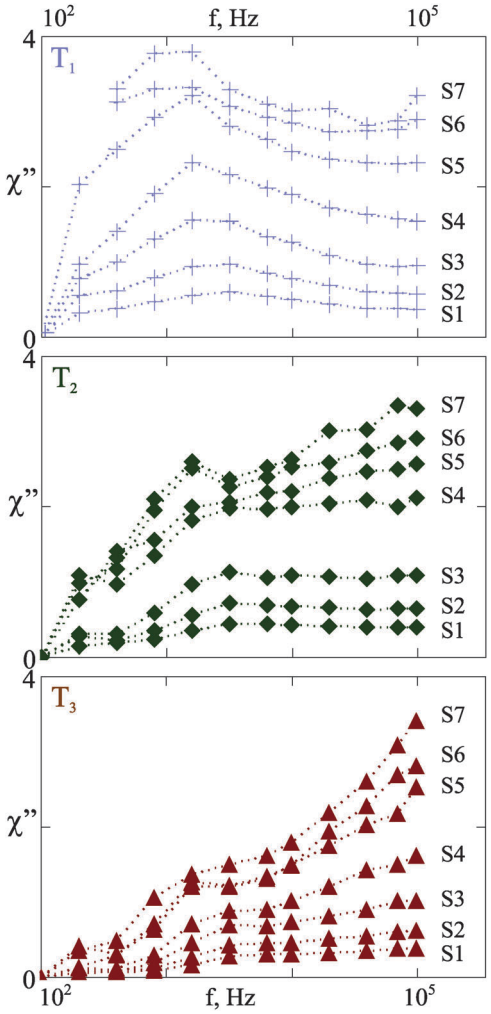

Fig. 7 Experimental results for the imaginary part of the dynamic zero-field susceptibility for samples S1–S7 (as indicated in each curve) at different temperatures T_1–T_3 shown in the upper left corners.

presence of highly correlated and weakly responsive structures, rather than individual particles with Brownian magnetic relaxation corresponding to 10^{-2} s ($x > 19$ nm), whose molar portion obtained from $p(x)$, shown in the inset of Fig. 2, is below 1%.

In the upper plot of Fig. 7, $T = T_1$, one can see that for all samples the value of χ'' at frequencies of about 10^5 Hz is lower than that in the range 10^3–10^4 Hz. This changes, however, with increasing temperature. Thus, already at T_2 this trend is inverted and at T_3 the low-f maximum is basically replaced by a plateau, especially for low concentrated samples S1–S3. It means that the structures, formed at low T, release the particles on heating, and the latter become less correlated. This effect becomes smaller with decreasing nanoparticle concentration. From the three temperature plots in Fig. 7, one can conclude the temperature at which the correlated structures are formed. For our samples it occurs between 240 and 250 K. This interval can be determined by comparing the low-f maximum value to the values at $f = 10^5$ Hz at T_1 and T_2. At the same time, the lifetime of these correlated structures is not sufficient enough to affect the static magnetic response of the samples. Finally, it is crucial to underline that the carrier remains liquid in the complete range of studied temperatures.

5 Conclusions

In this paper, we present a combined experimental and theoretical study aimed at analysing the dynamic zero-field susceptibility of magnetic nanoparticle suspensions. A specific feature of magnetic nanoparticles suspended in a liquid carrier is that they can exhibit various magnetic relaxations depending on their size. Thus, the polydisperse system is expected to respond to the AC fields in a unique way depending on the particle size distribution. On the other hand, the inherent magnetic interparticle correlations, which change with temperature and nanoparticle concentration, cannot but affect the dynamics of the system and might lead to a qualitative change in the response. In order to carefully separate all these dependencies, we obtained seven samples with an identical particle size distribution different only in the nanoparticle volume fraction by using a basic sample. The particle size distribution was first defined by magnetogranulometry based on static magnetic measurements and then verified comparing a reliable theoretical model (MMF2) to the initial static zero-field susceptibility measured for all the seven samples. As a next step, we measured dynamic zero-field complex susceptibility at five different temperatures in the range of almost 100 K for all samples. The response we obtained for different nanoparticle concentrations turned out to be qualitatively similar and showed a very strong temperature dependence. Here, it is worth mentioning that the carrier remained liquid in all the experiments. At high temperatures, the real part of the spectra of the magnetic response remains basically constant, and the imaginary parts show almost no maxima in the investigated frequency range (10–10^5 Hz). This clearly changes at lower temperatures, at which the real part shows a rapid decrease at rather low frequencies (10^2 Hz), and the low frequency maximum starts being clearly observable. In order to elucidate the physical origin of this behaviour at low concentrations, we applied an earlier developed mean-field approach,[73] in which the dipolar correlations are accurately considered. Apart from finding a very good agreement between our theoretical approach and the experimental data for dilute samples, we also managed to show how, in this concentration range, the magnetic correlations determine the dynamic response, which is clearly different from the Debye superposition of individual nanoparticle magnetic relaxations. Beyond the mean-field limit, when the concentrations of magnetic nanoparticles are high and the temperature is low, we perform a thorough analysis of the dynamic spectra, extensively comparing them to the individual particle relaxation times. This allows us to conclude that the slow response cannot be attributed to a very small fraction of large magnetic nanoparticles, but is rather caused by the presence of large particle structures in which magnetic moments are very strongly correlated and cannot react fast enough to the externally applied magnetic field. However, the

correlations in this parameter range are dynamic and their signature cannot be found in the static magnetic response. This unique combination of competing individual relaxations accompanied by the presence of temperature and concentration dependent correlations can be observed to such a large extent in the systems only of superparamagnetic nanoparticles. This also provides the basis for various applications of such suspensions in medicine, nanotechnology and microfluidics.[112–118] Thus, we believe that a deeper understanding of the dynamic correlated structure formed in the suspensions of magnetic nanoparticle suspensions opens up new perspectives in tuning and controlling their magnetic behaviour in AC fields.

Acknowledgements

The research was supported by Russian Science Foundation Grant (No. 15-12-10003). S. S. K. is grateful to the FWF START-Project Y 627-N27 and EU-Project 642774 ETN-Colldense. We also thank Michaela McCaffrey for language corrections.

References

1 J. Dobson, *Nanomedicine*, 2006, **1**, 31–37.
2 J. Durán, J. Arias, V. Gallardo and A. Delgado, *J. Pharm. Sci.*, 2008, **97**, 2948–2983.
3 S. Hughes, S. McBain, J. Dobson and A. J. El Haj, *J. R. Soc., Interface*, 2008, **5**, 855–863.
4 Q. A. Pankhurst, N. T. K. Thanh, S. K. Jones and J. Dobson, *J. Phys. D: Appl. Phys.*, 2009, **42**, 224001.
5 D. Ortega, N. Perez, J. L. Vilas, J. S. Garitaonandia, K. Suzuki, J. R. Marin and M. Rodriguez, *J. Appl. Phys.*, 2013, **113**, 17B505.
6 E. Pollert, G. Goglio, S. Mornet and E. Duguet, *Nanomaterials: A Danger or a Promise?*, Springer London, 2013, pp. 99–129.
7 J. L. F. Gabayno, D.-W. Liu, M. Chang and Y.-H. Lin, *Nanoscale*, 2015, **7**, 3947–3953.
8 J. Hong, P. Purwar, M. Cha and J. Lee, *Nanoscale*, 2015, **7**, 19110–19117.
9 F. Kremer and A. Schönhals, *Broadband Dielectric Spectroscopy*, 2003.
10 L. P. Singh and R. Richert, *Phys. Rev. Lett.*, 2012, **109**, 167802.
11 Z. Wojnarowska, Y. Wang, J. Pionteck, K. Grzybowska, A. P. Sokolov and M. Paluch, *Phys. Rev. Lett.*, 2013, **111**, 225703.
12 M. Sega, S. S. Kantorovich, A. Arnold and C. Holm, *Recent Advances in Broadband Dielectric Spectroscopy*, Springer Netherlands, 2013, pp. 103–122.
13 M. Sega, S. S. Kantorovich, C. Holm and A. Arnold, *J. Chem. Phys.*, 2014, **140**, 211101.
14 V. Raicu and Y. Feldman, *Dielectric Relaxation in Biological Systems: Physical Principles, Methods, and Applications*, 2015.
15 A. Pshenichnikov and A. Lebedev, *Soviet Physics, JETP (English Translation)*, 1989, **68**, 498–502.
16 B. H. Erné, K. Butter, B. W. M. Kuipers and G. J. Vroege, *Langmuir*, 2003, **19**, 8218–8225.
17 S. H. Chung, A. Hoffmann, S. D. Bader, C. Liu, B. Kay, L. Makowski and L. Chen, *Appl. Phys. Lett.*, 2004, **85**, 2971–2973.
18 R. Ferguson, A. Khandhar, C. Jonasson, J. Blomgren, C. Johansson and K. Krishnan, *Magnetics, IEEE Transactions on*, 2013, **49**, 3441–3444.
19 C. Moya, O. Iglesias-Freire, X. Batlle, A. Labarta and A. Asenjo, *Nanoscale*, 2015, **7**, 17764–17770.
20 M. Estrader, A. Lopez-Ortega, I. V. Golosovsky, S. Estrade, A. G. Roca, G. Salazar-Alvarez, L. Lopez-Conesa, D. Tobia, E. Winkler, J. D. Ardisson, W. A. A. Macedo, A. Morphis, M. Vasilakaki, K. N. Trohidou, A. Gukasov, I. Mirebeau, O. L. Makarova, R. D. Zysler, F. Peiro, M. D. Baro, L. Bergstrom and J. Nogues, *Nanoscale*, 2015, **7**, 3002–3015.
21 S. Sacanna, L. Rossi, B. W. M. Kuipers and A. P. Philipse, *Langmuir*, 2006, **22**, 1822–1827.
22 M. Nakade, T. Ikeda and M. Ogawa, *J. Mater. Sci.*, 2007, **42**, 4815–4823.
23 G. Liu, L. Li and X. Yang, *Polymer*, 2008, **49**, 4776–4783.
24 T. Klein, A. Laptev, A. Gunther, P. Bender, A. Tschope and R. Birringer, *J. Appl. Phys.*, 2009, **106**, 114301.
25 M. Yan, J. Fresnais and J.-F. Berret, *Soft Matter*, 2010, **6**, 1997–2005.
26 A. Günther, P. Bender, A. Tschöpe and R. Birringer, *J. Phys.: Condens. Matter*, 2011, **23**, F5103.
27 C. E. Alvarez and S. H. L. Klapp, *Soft Matter*, 2012, **8**, 7480–7489.
28 S. Kantorovich, E. Pyanzina and F. Sciortino, *Soft Matter*, 2013, **9**, 6594–6603.
29 J. Mohapatra, A. Mitra, H. Tyagi, D. Bahadur and M. Aslam, *Nanoscale*, 2015, **7**, 9174–9184.
30 L. Rossi, S. Sacanna, W. T. M. Irvine, P. M. Chaikin, D. J. Pine and A. P. Philipse, *Soft Matter*, 2011, **7**, 4139–4142.
31 J. G. Donaldson and S. S. Kantorovich, *Nanoscale*, 2015, **7**, 3217–3228.
32 L. Wu, B. Shen and S. Sun, *Nanoscale*, 2015, **7**, 16165–16169.
33 L. T. Lu, N. T. Dung, L. D. Tung, C. T. Thanh, O. K. Quy, N. V. Chuc, S. Maenosono and N. T. K. Thanh, *Nanoscale*, 2015, **7**, 19596–19610.
34 A. Demortiere, P. Panissod, B. P. Pichon, G. Pourroy, D. Guillon, B. Donnio and S. Begin-Colin, *Nanoscale*, 2011, **3**, 225–232.
35 G. Muscas, N. Yaacoub, G. Concas, F. Sayed, R. Sayed Hassan, J. M. Greneche, C. Cannas, A. Musinu, V. Foglietti, S. Casciardi, C. Sangregorio and D. Peddis, *Nanoscale*, 2015, **7**, 13576–13585.
36 B. Ren, A. Ruditskiy, J. H. K. Song and I. Kretzschmar, *Langmuir*, 2012, **28**, 1149–1156.
37 I. Kretzschmar, S. Gangwal, A. B. Pawar and O. D. Velev, *Janus particle synthesis, self-assembly and applications*, The Royal Society of Chemistry, New York, 2012, pp. 168–203.
38 A. Ruditskiy, B. Ren and I. Kretzschmar, *Soft Matter*, 2013, **9**, 9174–9181.

39 P. Granitzer, K. Rumpf, R. Gonzalez-Rodriguez, J. L. Coffer and M. Reissner, *Nanoscale*, 2015, **7**, 20220–20226.
40 C. Stotzel, H.-D. Kurland, J. Grabow and F. A. Muller, *Nanoscale*, 2015, **7**, 7734–7744.
41 G. Steinbach, D. Nissen, M. Albrecht, E. V. Novak, P. A. Sanchez, S. S. Kantorovich, S. Gemming and A. Erbe, *Soft Matter*, 2016, **12**, 2737–2743.
42 M. E. Hayden and U. O. Häfeli, *J. Phys.: Condens. Matter*, 2006, **18**, S2877.
43 C. S. Brazel, *Pharm. Res.*, 2009, **26**, 644–656.
44 K. M. Krishnan, *Magnetics, IEEE Transactions on*, 2010, **46**, 2523–2558.
45 M. M. van Oene, L. E. Dickinson, F. Pedaci, M. Köber, D. Dulin, J. Lipfert and N. H. Dekker, *Phys. Rev. Lett.*, 2015, **114**, 218301.
46 R. Hergt, R. Hiergeist, I. Hilger, W. Kaiser, Y. Lapatnikov, S. Margel and U. Richter, *J. Magn. Magn. Mater.*, 2004, **270**, 345–357.
47 F. Sonvico, S. Mornet, S. Vasseur, C. Dubernet, D. Jaillard, J. Degrouard, J. Hoebeke, E. Duguet, P. Colombo and P. Couvreur, *Bioconjugate Chem.*, 2005, **16**, 1181–1188.
48 J.-P. Fortin, C. Wilhelm, J. Servais, C. Ménager, J.-C. Bacri and F. Gazeau, *J. Am. Chem. Soc.*, 2007, **129**, 2628–2635.
49 A. Espinosa, M. Bugnet, G. Radtke, S. Neveu, G. A. Botton, C. Wilhelm and A. Abou-Hassan, *Nanoscale*, 2015, **7**, 18872–18877.
50 R. A. Bohara, N. D. Thorat, A. K. Chaurasia and S. H. Pawar, *RSC Adv.*, 2015, **5**, 47225–47234.
51 C. A. Quinto, P. Mohindra, S. Tong and G. Bao, *Nanoscale*, 2015, **7**, 12728–12736.
52 R. Müller, R. Hergt, M. Zeisberger and W. Gawalek, *J. Magn. Magn. Mater.*, 2005, **289**, 13–16.
53 Y. L. Raikher and V. Stepanov, *J. Magn. Magn. Mater.*, 2014, **368**, 421–427.
54 M. Boskovic, G. F. Goya, S. Vranjes-Djuric, N. Jovic, B. Jancar and B. Antic, *J. Appl. Phys.*, 2015, **117**, 103903.
55 Y. L. Raikher and V. I. Stepanov, *Nonlinear Dynamic Susceptibilities and Field-Induced Birefringence in Magnetic Particle Assemblies*, John Wiley and Sons Inc., 2004, pp. 419–588.
56 A. Ivanov, S. Kantorovich, E. Reznikov, C. Holm, A. Pshenichnikov, A. Lebedev, A. Chremos and P. Camp, *Phys. Rev. E: Stat., Nonlinear, Soft Matter Phys.*, 2007, **75**, 061405.
57 J. Köfinger and C. Dellago, *Phys. Rev. Lett.*, 2009, **103**, 080601.
58 D. Heinrich, A. R. Goñi, A. Smessaert, S. H. L. Klapp, L. M. C. Cerioni, T. M. Osán, D. J. Pusiol and C. Thomsen, *Phys. Rev. Lett.*, 2011, **106**, 208301.
59 M. Klokkenburg, R. Dullens, W. Kegel, B. Erné and A. Philipse, *Phys. Rev. Lett.*, 2006, **96**, 037203.
60 S. Kantorovich, A. O. Ivanov, L. Rovigatti, J. M. Tavares and F. Sciortino, *Phys. Rev. Lett.*, 2013, **110**, 148306.
61 A. Y. Zubarev and A. V. Yushkov, *J. Exp. Theor. Phys*, 1998, **87**, 484.
62 B. U. Felderhof and R. B. Jones, *J. Phys.: Condens. Matter*, 2003, **15**, 4011.
63 P. Ilg and S. Hess, *Zeitschrift für Naturforschung A*, 2003, **58**, 589–600.
64 P. M. Déjardin and F. Ladieu, *J. Chem. Phys.*, 2014, **140**, 034506.
65 E. L. Verde, G. T. Landi, J. A. Gomes, M. H. Sousa and A. F. Bakuzis, *J. Appl. Phys.*, 2012, **111**, 123902.
66 M. A. Martens, R. J. Deissler, Y. Wu, L. Bauer, Z. Yao, R. Brown and M. Griswold, *Med. Phys.*, 2013, **40**, 022303.
67 G. T. Landi, *Phys. Rev. B: Condens. Matter Mater. Phys.*, 2014, **89**, 014403.
68 M. Campanini, R. Ciprian, E. Bedogni, A. Mega, V. Chiesi, F. Casoli, C. de Julian Fernandez, E. Rotunno, F. Rossi, A. Secchi, F. Bigi, G. Salviati, C. Magen, V. Grillo and F. Albertini, *Nanoscale*, 2015, **7**, 7717–7725.
69 P. Morais, L. Silveira, A. Oliveira and J. Santos, *Rev. Adv. Mater. Sci.*, 2008, **18**, 536–540.
70 M. Vasilakaki, C. Binns and K. N. Trohidou, *Nanoscale*, 2015, **7**, 7753–7762.
71 M. S. Carriao and A. F. Bakuzis, *Nanoscale*, 2016, **8**, 8363–8377.
72 C. Munoz-Menendez, I. Conde-Leboran, D. Baldomir, O. Chubykalo-Fesenko and D. Serantes, *Phys. Chem. Chem. Phys.*, 2015, **17**, 27812–27820.
73 A. O. Ivanov, V. S. Zverev and S. S. Kantorovich, *Soft Matter*, 2016, **12**, 3507–3513.
74 J. O. Sindt, P. J. Camp, S. S. Kantorovich, E. A. Elfimova and A. O. Ivanov, *Phys. Rev. E: Stat., Nonlinear, Soft Matter Phys.*, 2016, in press.
75 R. E. Rosensweig, *Ferrohydrodynamics*, Cambridge Univ. Press, Cambridge, 1985.
76 S. W. Charles, *Ferrofluids: Magnetically Controllable Fluids and Their Applications*, Springer, Berlin, Germany, 2002, vol. 594, pp. 3–18.
77 A. Pshenichnikov, V. Mekhonoshin and A. Lebedev, *J. Magn. Magn. Mater.*, 1996, **161**, 94–102.
78 A. Pshenichnikov, A. Lebedev and K. Morozov, *Magnetohydrodynamics*, 1987, **23**, 31–36.
79 A. F. Pshenichnikov, *Instrum. Exp. Tech.*, 2007, **50**, 509–514.
80 E. Blums, A. Cebers and M. M. Maiorov, *Magnetic Fluids*, W. de Gruyter, Berlin, 1997.
81 P. Langevin, *J. de Phys.*, 1905, **4**, 678.
82 P. Langevin, *Ann. Chim. et Phys.*, 1905, **5**, 70.
83 M. S. Wertheim, *J. Stat. Phys.*, 1984, **35**, 19–34.
84 M. S. Wertheim, *J. Stat. Phys.*, 1986, **42**, 477–492.
85 B. M. Berkovskii, V. I. Kalikmanov and V. S. Filinov, *Magnetohydrodynamics*, 1987, **23**, 150–157.
86 M. Holmes, K. O'Grady and J. Popplewell, *J. Magn. Magn. Mater.*, 1990, **85**, 47–50.
87 M. Shliomis, A. Pshenichnikov, K. Morozov and I. Shurubor, *J. Magn. Magn. Mater.*, 1990, **85**, 40–46.
88 Y. A. Buyevich and A. O. Ivanov, *Physica A*, 1992, **190**, 276.
89 A. F. Pshenichnikov, *J. Magn. Magn. Mater.*, 1995, **145**, 319–326.
90 D. Henderson, D. Boda, I. Szalai and K.-Y. Chan, *J. Chem. Phys.*, 1999, **110**, 7348–7353.
91 B. Huke and M. Lücke, *Phys. Rev. E: Stat. Phys., Plasmas, Fluids, Relat. Interdiscip.*, 2000, **62**, 6875–6890.

92 A. O. Ivanov and O. B. Kuznetsova, *Phys. Rev. E: Stat., Nonlinear, Soft Matter Phys.*, 2001, **64**, 041405.
93 B. Huke and M. Lücke, *J. Magn. Magn. Mater.*, 2002, **252**, 132–134.
94 B. Huke and M. Lücke, *Phys. Rev. E: Stat., Nonlinear, Soft Matter Phys.*, 2003, **67**, 051403.
95 K. I. Morozov, *J. Chem. Phys.*, 2007, **126**, 194506.
96 E. A. Elfimova, A. O. Ivanov and P. J. Camp, *Phys. Rev. E: Stat., Nonlinear, Soft Matter Phys.*, 2012, **86**, 021126.
97 I. Szalai, S. Nagy and S. Dietrich, *J. Phys.: Condens. Matter*, 2013, **25**, 465108.
98 I. Szalai, S. Nagy and S. Dietrich, *Phys. Rev. E: Stat., Nonlinear, Soft Matter Phys.*, 2015, **92**, 042314.
99 A. O. Ivanov and O. B. Kuznetsova, *Colloid J.*, 2006, **68**, 430–440.
100 A. F. Pshenichnikov and A. V. Lebedev, *J. Chem. Phys.*, 2004, **121**, 5455–5467.
101 A. F. Pshenichnikov and A. V. Lebedev, *Colloid J.*, 2005, **67**, 189–200.
102 M. Martsenyuk, Y. L. Raikher and M. Shliomis, *JETP*, 1974, **38**, 413.
103 M. I. Shliomis and V. I. Stepanov, *Theory of the Dynamic Susceptibility of Magnetic Fluids*, John Wiley and Sons, Inc., 2007, pp. 1–30.
104 W. Coffey, P. Cregg, D. Crothers, J. Waldron and A. Wickstead, *J. Magn. Magn. Mater.*, 1994, **131**, L301–L303.
105 W. F. Brown, *Phys. Rev.*, 1963, **130**, 1677–1686.
106 S. Vonsovsky, *Magnetism*, Johh Wiley and Sons, New York, 1974.
107 L. R. Bickford, J. Pappis and J. L. Stull, *Phys. Rev.*, 1955, **99**, 1210–1214.
108 P. Debye, *Ver. Deut. Phys. Gesell.*, 1913, **15**, 777.
109 L. Rovigatti, J. Russo and F. Sciortino, *Phys. Rev. Lett.*, 2011, **107**, 237801.
110 L. Rovigatti, J. Russo and F. Sciortino, *Soft Matter*, 2012, **8**, 6310–6319.
111 S. S. Kantorovich, A. O. Ivanov, L. Rovigatti, J. M. Tavares and F. Sciortino, *Phys. Chem. Chem. Phys.*, 2015, **17**, 16601–16608.
112 X. Liu, L. Fu, S. Hong, V. Dravid and C. Mirkin, *Adv. Mater.*, 2002, **14**, 231–234.
113 M. A. M. Gijs, *Microfluidics and Nanofluidics*, 2004, **1**, 22–40.
114 F. Fahrni, M. Prins and L. van IJzendoorn, *J. Magn. Magn. Mater.*, 2009, **321**, 1843–1850.
115 P. Qu, J. Lei, L. Zhang, R. Ouyang and H. Ju, *J. Chromatogr. A*, 2010, **1217**, 6115–6121.
116 C. Barrera, V. Florian-Algarin, A. Acevedo and C. Rinaldi, *Soft Matter*, 2010, **6**, 3662–3668.
117 S. van Berkum, J. T. Dee, A. P. Philipse and B. H. Erne, *International Journal of Molecular Sciences*, 2013, **14**, 10162.
118 F. Pineux, R. Marega, A. Stopin, A. La Torre, Y. Garcia, E. Devlin, C. Michiels, A. N. Khlobystov and D. Bonifazi, *Nanoscale*, 2015, **7**, 20474–20488.

